Critical behavior of the ferromagnetic transition in GdSc(Si,Ge) intermetallic compounds

A. Herrero[a], A. Oleaga [a],*, P. Manfrinetti [b,c], A. Provino [b,c], A. Salazar [a]

[a] Departamento de Física Aplicada I, Escuela de Ingeniería de Bilbao, Universidad del País Vasco UPV/EHU, Plaza Ingeniero Torres Quevedo 1, 48013 Bilbao, Spain

[b] Department of Chemistry, University of Genova, Via Dodecaneso 31, Genova 16146, Italy

[c] Institute SPIN-CNR, Corso Perrone 24, 16152 Genova, Italy

ABSTRACT

A complete study on the critical behavior of the paramagnetic to ferromagnetic transition in intermetallics GdScSi, GdScGe, GdSc(Si$_{0.5}$Ge$_{0.5}$) and Gd(Sc$_{0.5}$Ti$_{0.5}$)Ge has been carried out by means of magnetic as well as calorimetric measurements, using a high resolution *ac* photopyroelectric technique. The critical exponents α, β, γ, δ and the ratio of the critical coefficients A^+/A^- have been independently obtained for the four samples. It has been proved that the magnetic interactions are short range as the values of the critical parameters correspond to the 3D-Heisenberg class, stating an isotropic ordering of the Gd spins. In some cases, there are small deviations of some of the critical parameters from the theoretical values which have been discussed on the basis of the variation of the *d* states hybridization between the rare earth and the transition metal, as well as the presence of small magnetocrystalline anisotropies arising from spin-orbit coupling effects.

Keywords: GdScSi; GdScGe; Spin-ordering; Thermal properties; Critical behavior; Ferromagnetism

* Corresponding author; E-mail address: *alberto.oleaga@ehu.es*

1. Introduction

Ternary intermetallic systems R-T-X (R = rare earth, T = transition metal, X = p-block element) are being extensively studied as promising magnetic systems for technological applications, specially due to the high temperature of their magnetic transitions. This makes them suitable candidates to look into the possibility of presenting strong magnetocaloric effects [1]. To this end, a knowledge as broad as possible of their properties (crystallographic as well as magnetic) is desirable. In particular, some extensive studies have already been undertaken on RScSi, RScGe, RTiSi, RTiGe (R = Ce, Pr, Nd, Sm, Gd, Tb, Dy, Ho, Er, Y) [2-14]; however, but there is an aspect which has been seldom studied up to now, and this is the critical behavior of the magnetic transitions, which gives valuable information about the range and dimensionality of the magnetic exchange interactions, together with the role that other mechanisms can play if the critical parameters obtained do not match a particular universality class. The knowledge of the variations of the universality class (which is tantamount to the physical mechanisms involved) with R, with T or with X (even with admixtures of T, X) will have to be taken into account when designing compositions in search of a strong magnetocaloric material.

Scaling analysis within the framework of renormalization group theory has established that the critical behavior of second order phase transitions in the near vicinity of the critical temperature T_C is characterized by a set of critical exponents α, β, γ, δ... associated with different thermal and magnetic properties, with interrelated values [15]. Each set of exponents (grouped in universality classes) is the result of proposing a different Hamiltonian to describe the physical system. For ferromagnetic materials, the most common universality classes with the corresponding values of the critical exponents are shown in Table 1 [16-19]. If long-range interactions are at the core of the magnetic interactions, the mean-field model should be the right one. The other three classes involve short-range order interactions: the Heisenberg model corresponds to an isotropic ferromagnetic material, XY model implies an easy-plane ferromagnetism while the Ising model is related to uniaxial anisotropy of the spins.

The critical exponent α is associated to the specific heat,

$$c_p(T) \quad \sim \quad A^{\pm} |t|^{-\alpha} \quad \text{(A$^-$ for $T < T_C$, A^+ for $T > T_C$)} \tag{1}$$

as a function of the reduced temperature $t = (T-T_C)/T_C$; this equation holds in the close vicinity of the critical temperature. On the other hand, β, γ and δ are associated with magnetic variables: the spontaneous magnetization (M_S), the inverse of initial susceptibility (χ_0^{-1}) and the critical isotherm, respectively:

$$M_S(T) \quad \sim \quad |t|^{\beta} \qquad (T < T_C), \tag{2}$$

$$\chi_0^{-1}(T) \quad \sim \quad |t|^{\gamma} \qquad (T > T_C), \tag{3}$$

$$M(H) \quad \sim \quad H^{1/\delta} \qquad (T = T_C). \tag{4}$$

The critical exponents are also involved in the magnetic equation of state in the critical region, which is given by

$$M (H, t) = |t|^{\beta} f_{\pm}(H/|t|^{\beta+\gamma}) \qquad (5)$$

where f_- and f_+ are regular analytic functions for $T < T_C$ and $T > T_C$, respectively.

In this study we are focusing our attention on some Gd members of this family, as they have the highest Curie temperature, slightly above room temperature, which make them good candidates for technological applications. We are presenting a complete study of the critical exponents (α, β, γ and δ) for the GdScSi, GdScGe, GdSc($Si_{0.5}Ge_{0.5}$), Gd($Sc_{0.5}Ti_{0.5}$)Ge compounds, in order to acknowledge whether, and how, a change in either the p-block element or the transition metal can alter their critical behavior.

2. Materials and Methods

Small samples of the ternary and pseudo-ternary compounds Gd(Sc,Ti)(Si,Ge), in form of polycrystalline alloys, were prepared and utilized in this work. The starting materials were high purity elements supplied by commercial vendors: 99.9 wt.% for both Gd and Sc (R metals from Koch-Light, England), 99.99+ wt.% Ti (from Aldrich Chem. USA), and 99.9999 wt.% for Si and Ge (from Alfa-Aesar, Germany). The alloys were prepared by arc melting stoichiometric amounts of the elements under a pure argon atmosphere on a water-cooled copper hearth; after a first melting and reaction of elements, the buttons were re-melted four times (turning them upside-down each time) to ensure homogenization (total weight of about 2 g; weight loss lower than 0.2 wt.%). The final alloys were placed inside an outgassed Ta tube, sealed under vacuum in silica tubes and annealed at 1000 °C for 10 days. Phase analysis, to check for quality of the samples was performed by X-ray powder diffraction using a Guinier camera [Cu Kα1 radiation; Si as internal standard (a= 5.4308(1) Å] and optical microscopy. Indexing of the powder diffraction patterns was carried out by comparison with the pattern calculated by the help of the Lazy-Pulverix program [20]; then, the lattice parameters calculated by least-squares fit. The alloys, prepared as above, resulted to be practically single phase: in the two samples containing Si only a 2-3 Vol.% of $Gd_{5-x}Sc_xSi_3$ (Mn_5Si_3-type) was present as secondary phase, while in the other two containing Ge the homologous phase $Gd_{5-x}Sc_xGe_3$ [21] was not even detectable (from Guinier pattern and as grain separation in the micrographic specimens).

Magnetization (M) measurements have been carried out in a VSM (Vibrating Sample Magnetometer) by Cryogenic Limited under external applied magnetic fields H_a ranging from 0 to 80 kOe. In order to completely cover the critical region, isotherms have been collected over a range of about ± 30 K around T_C (ΔT = 1 K). The applied magnetic field H_a has been corrected for demagnetization effects and the internal field calculated using the relation $H_i = H_a - NM$, where M is

the measured magnetization and N the demagnetization factor. This demagnetization factor has been obtained using the method given in references [22, 23], measuring the zero-field ac susceptibility. The so obtained H_i has been the one used for the scaling analysis. The magnetic susceptibility was measured with AC Measurement System Option in PPMS (Physical Properties Measurement System) by Quantum Design.

A high resolution *ac* photopyroelectric calorimeter in the back detection configuration has been used for the thermal measurements. Both thermal diffusivity and specific heat have been obtained for each of the four samples as a function of temperature in the region around the Curie temperature. This technique is very well suited to study the critical behavior in phase transitions and has been successfully applied to liquid crystals and solids (magnetic as well as ferroelectric transitions), including other intermetallic families [24-32]. The details of the experimental setup, as well as of the theory explaining how to retrieve the thermal variables from the photopyroelectric signal, can be found elsewhere [24, 33].

3. Experimental results and data fittings

The thermal diffusivity as a function of temperature for the four samples is shown in Fig. 1, from room temperature up to approximately 380 K. In all cases, the ferromagnetic phase transition is marked as a dip which alters the monotonic decrease from high temperatures to lower ones which is characteristic of intermetallic materials when there is no phase transition [34, 35]. In other members of the same intermetallic family (NdScSi, NdScGe) with ferromagnetic transitions, the same behavior and dip have been observed [32]. This kind of dip signaling a ferromagnetic transition is common in many other magnetic materials, such as manganites [36, 37] but with the difference that in the latter, as thermal insulators, the thermal diffusivity monotonically increases while temperature is reduced. Starting from GdScGe, which has the higher values of thermal diffusivity, the substitution of Ge by 50% Si reduces somewhat the thermal diffusivity and slightly shifts the critical temperature to higher temperature while the shape of the dip is very similar. The total substitution of Ge by Si, on the other hand, shifts down the critical temperature about 15 K and makes the dip shallower, with a thermal diffusivity in general smaller than the one for GdScGe. Finally, the substitution of 50% Sc by Ti does introduce a big change in the general shape of the curve, reducing even more the thermal diffusivities values while shifting down the Curie temperature about 15 K.
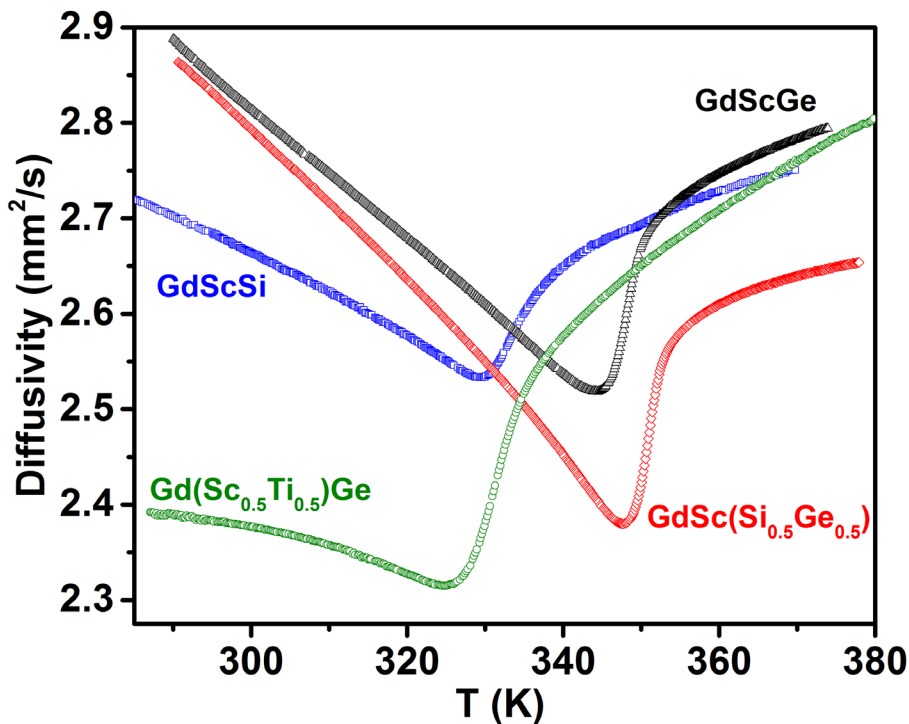

Fig. 1 Thermal diffusivity as a function of temperature for GdScSi (■), GdScGe (▲), GdSc(Si$_{0.5}$Ge$_{0.5}$) (♦), Gs(Sc$_{0.5}$Ti$_{0.5}$)Ge (●). Not all points are shown, for the sake of clarity.

Fig. 2 shows the magnetization per unit mass as a function of temperature for the four samples. All of them are very similar in shape, with the non-codoped samples GeScSi and GeScGe giving the higher values.
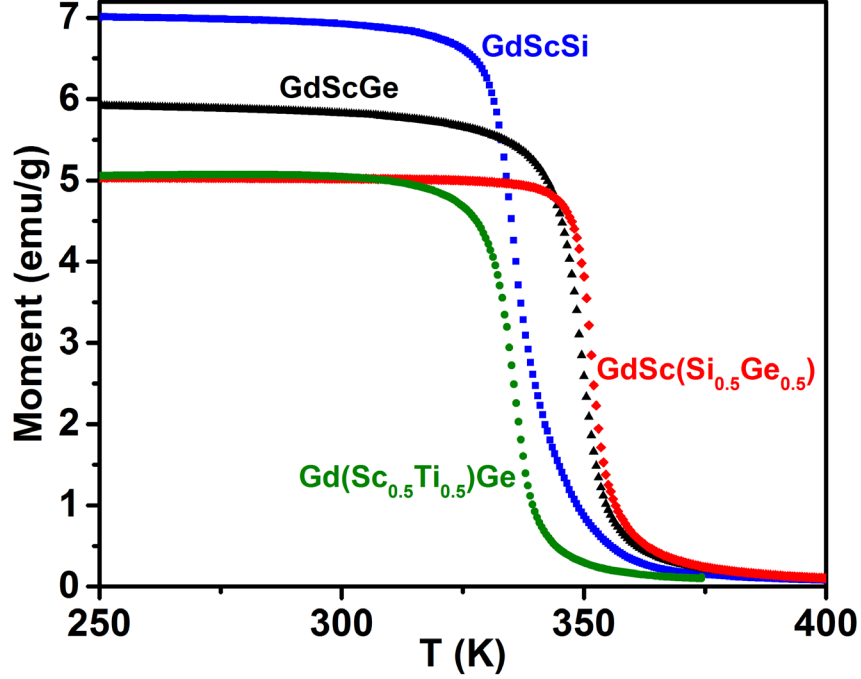

Fig. 2. Magnetization as a function of temperature for GdScSi (■), GdScGe (▲), GdSc(Si$_{0.5}$Ge$_{0.5}$) (♦), Gs(Sc$_{0.5}$Ti$_{0.5}$)Ge (●) using a magnetic field of 100 Oe.

In what follows we are going to present the scaling analysis of the four samples, in parallel. In the text and in the figures, H will mean the internal field H_i, to simplify the notation. The usual procedure is, first, to represent the standard Arrott Plot (M^2 as a function of H/M) for isotherms in an appropriate temperature range around the Curie temperature in each case (301-356 K for GdScSi, 316-374 K for GdScGe, 318-372 K for GdSc(Si$_{0.5}$Ge$_{0.5}$) and 301-360 K for Gd(Sc$_{0.5}$Ti$_{0.5}$)Ge. If long-range interactions were responsible for the ferromagnetic transition, there would be a linear behavior at high fields on that plot. Fig 3a contains the experimental points obtained for GdScGe in which it is clearly seen that this is not the case: the curves are not linear and all of them have a positive slope, the latter confirming the second order character of the transition after the Banerjee criterion [38], while the former discards a mean field behavior. The results for the other three samples present exactly the same behavior. Therefore, we have turned our attention to the so-called Modified Arrott Plots (MAP) as the next step, representing $M^{1/\beta}$ versus $(H/M)^{1/\gamma}$ for certain relevant universality classes, such as 3D-Heisenberg ($\beta = 0.365$, $\gamma = 1.386$) and 3D-Ising ($\beta = 0.3265$, $\gamma = 1.237$). Linear

fittings of the experimental points at high fields have been performed with the result that in both cases straight lines are obtained but much more parallel among them for the Heisenberg case than for the Ising one. Fig. 3b shows the particular case of the MAP with the Heisenberg values for GdScGe where it is clear that the fitting to straight lines is good and that they are visually parallel. This also happens in the other 3 samples, with graphs so alike that it is not worth showing them all. In order to quantify the parallelism and make a decision about the best one, we have calculated the deviation of the slopes for the Heisenberg and Ising cases for the four samples: $\approx \pm 7\%$ against $\approx \pm 16\%$ for GdScSi, $\approx \pm 5\%$ against $\approx \pm 16\%$ for GdScGe, $\approx \pm 4\%$ against $\approx \pm 14\%$ for $GdSc(Si_{0.5}Ge_{0.5})$, $\approx \pm 4\%$ against $\approx \pm 15\%$ for $Gd(Sc_{0.5}Ti_{0.5})Ge$.

Thus, in the four cases, the Heisenberg critical exponents have been taken as the first trial to refine them using the well known iteration procedure [39, 40]. A linear extrapolation of the isotherms in Fig. 3b has been taken from the high field values to extract $(M_S)^{1/\beta}$ and $(\chi_0^{-1})^{1/\gamma}$ as an intercept on $M^{1/\beta}$ and $(H/M)^{1/\gamma}$ axes, respectively. The so obtained values of $M_S(T)$ and $\chi_0^{-1}(T)$ have been independently fitted to Eqs. (2) and (3), respectively, thus extracting new values of β and γ. The process is repeated till convergence is reached and the best values of β, γ and T_C are obtained. The final values of $M_S(T)$ and $\chi_0^{-1}(T)$ are plotted as a function of temperature in Fig. 4 for the four compositions, while Table 2 contains all the critical exponents and temperatures obtained from the fittings. In the four cases, β agrees with the Heisenberg case, while γ exactly agrees for GdScSi and in the other three cases is slightly smaller, though in no case it takes a value as low as the one for the Ising case.

In order to determine β, γ and T_C with more accuracy, the Kouvel Fisher method has been applied [41] to the four samples, which assesses that $M_S(dM_S/dT)^{-1}$ and $\chi_0^{-1}(d\chi_0^{-1}/dT)^{-1}$ have a linear behavior with respect to T, with slopes $1/\beta$ and $1/\gamma$, respectively. The Curie temperature arises from the intercept of the straight fitted lines on the temperature axis. The four Kouvel Fisher plots are shown in Fig. 5 and the critical exponents obtained are grouped in Table 2. For each sample, both methods (MAP and Kouvel Fisher) give very similar values, confirming the reliability of the results.
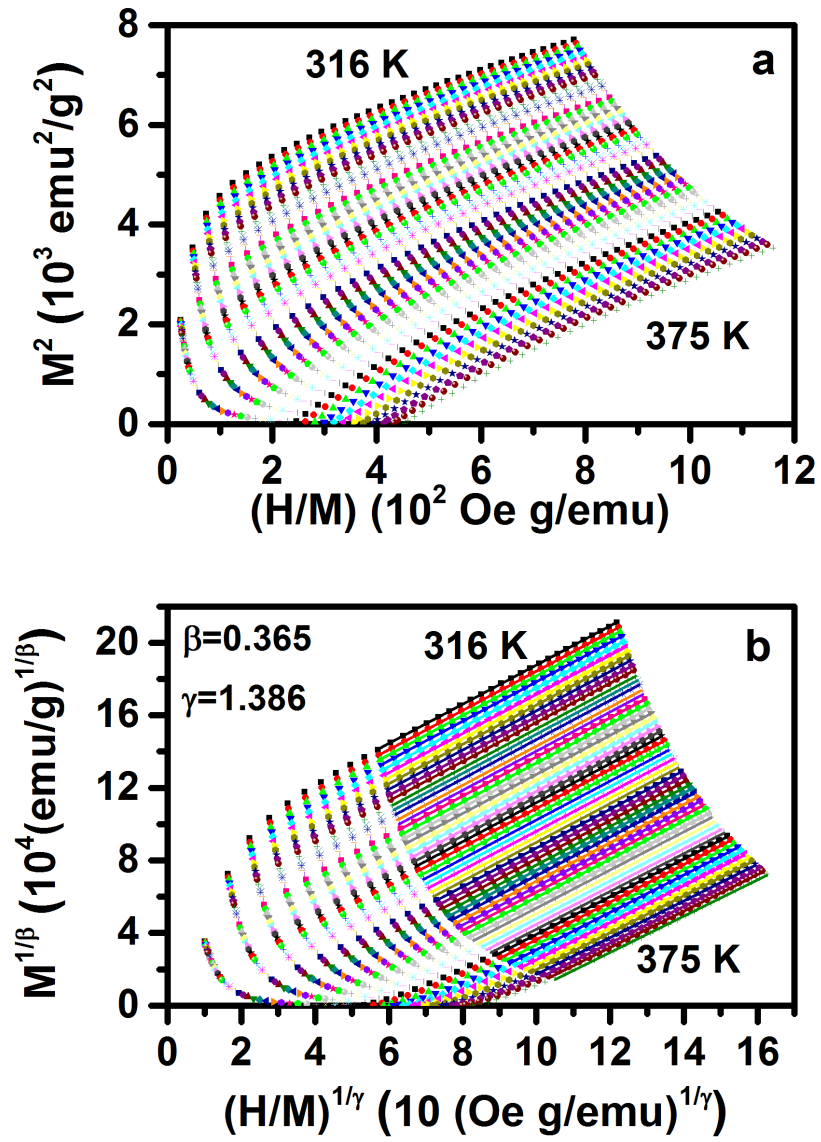
Fig. 3. (a) Arrott Plot and (b) Modified Arrott Plot of the isotherms collected around T_C for GdScGe, with the

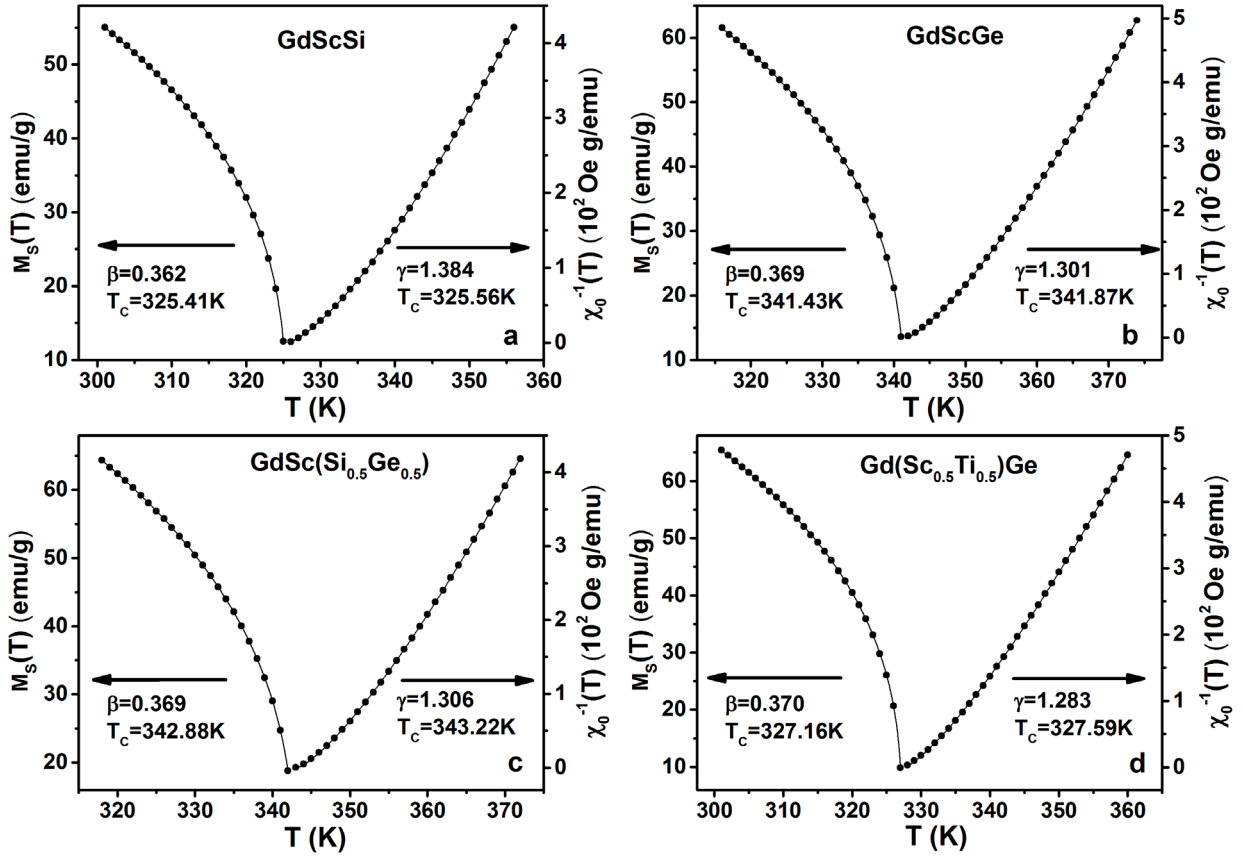Heisenberg trial exponents showing the parallelism of the linear fittings at high fields.

Fig.4. Spontaneous magnetization (left) and inverse of initial susceptibility (right) vs. temperature for GdScSi (a), GdScGe (b), GdSc(Si$_{0.5}$Ge$_{0.5}$) (c), Gd(Sc$_{0.5}$Ti$_{0.5}$)Ge (d), as obtained from the optimized Modified Arrot Plot. The solid curves correspond to the fits to Eq. (2) and (3), as explained in the text.
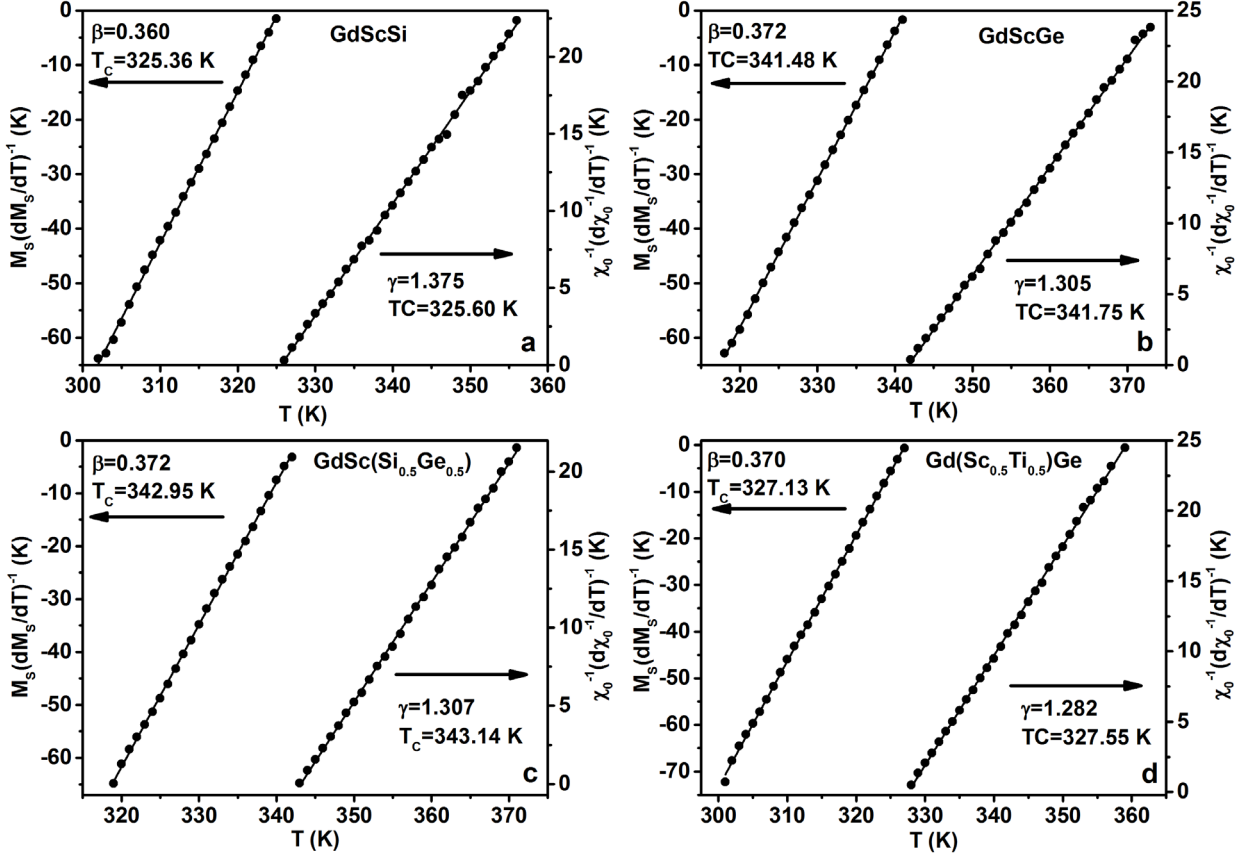
Fig. 5. Kouvel-Fisher plot of spontaneous magnetization (left) and inverse of initial susceptibility (right) for GdScSi (a), GdScGe (b), GdSc(Si$_{0.5}$Ge$_{0.5}$) (c), Gd(Sc$_{0.5}$Ti$_{0.5}$)Ge (d). The straight lines are linear fits, from which T$_C$ and the critical exponents are obtained.

The following magnetic critical exponent, δ, can be mathematically derived from the scaling law [15]

$$\delta = 1 + \gamma/\beta \qquad (6)$$

and experimentally obtained by means of Eq. (4), as well. Fig. 6 contains the critical isotherms at 325 K for GdScSi, 342 K for GdScGe, 343 K for GdSc(Si$_{0.5}$Ge$_{0.5}$) and 327 K for Gd(Sc$_{0.5}$Ti$_{0.5}$)Ge, all of them in log-log scale, showing that they are good straight lines whose slopes give the values for δ. The experimental values agree very well with the theoretical one and are very close to the ones obtained through the scaling law. All these results are also contained in Table 2.

The fulfillment of the magnetic equation of state Eq. (5), with the critical exponents β, γ just obtained, is considered as the most severe confirmation of a good scaling. Fig. 7 shows that, in the four cases, the results collapse extremely well into two independent branches, above and below T_C.
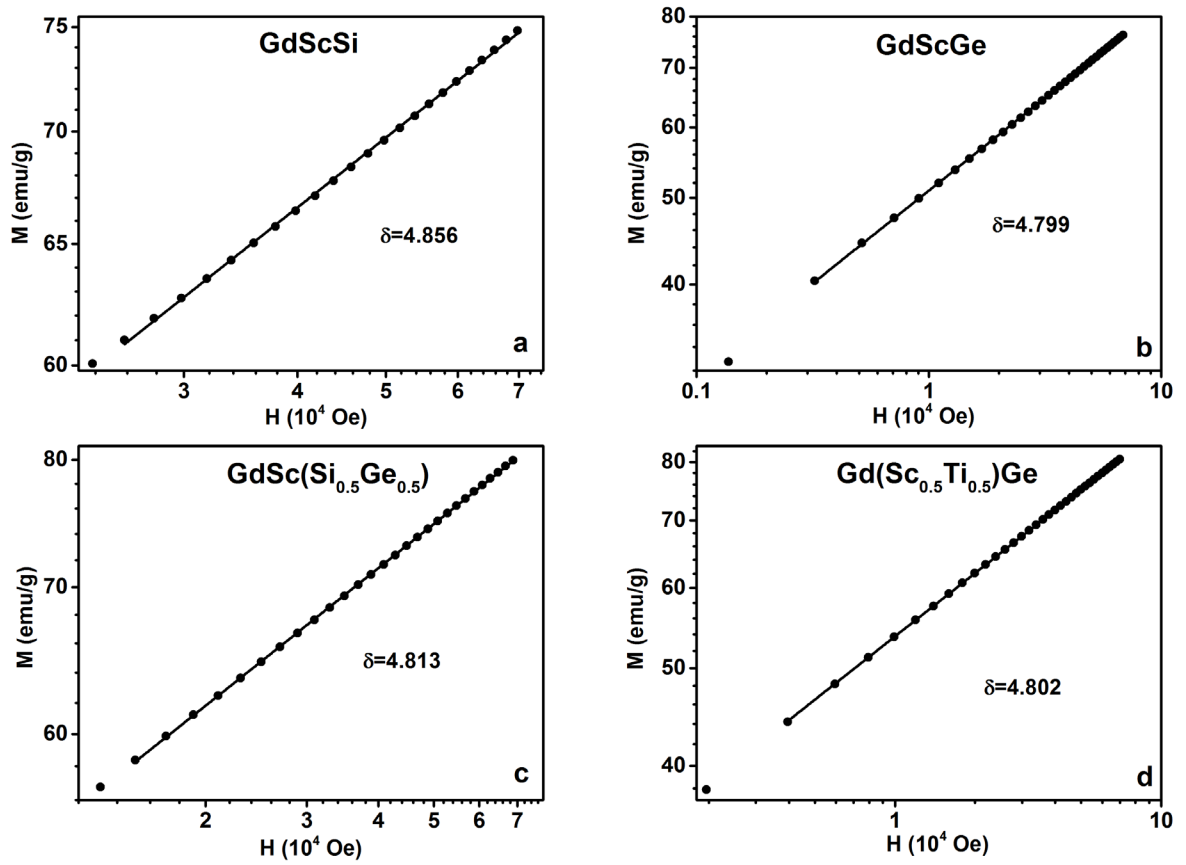
Fig. 6. *M* vs. *H* plot in a log-log scale collected at critical isotherms for GdScSi (a), GdScGe (b), GdSc(Si$_{0.5}$Ge$_{0.5}$) (c), Gd(Sc$_{0.5}$Ti$_{0.5}$)Ge (d). The straight line is the linear fit from which the exponent δ is obtained.
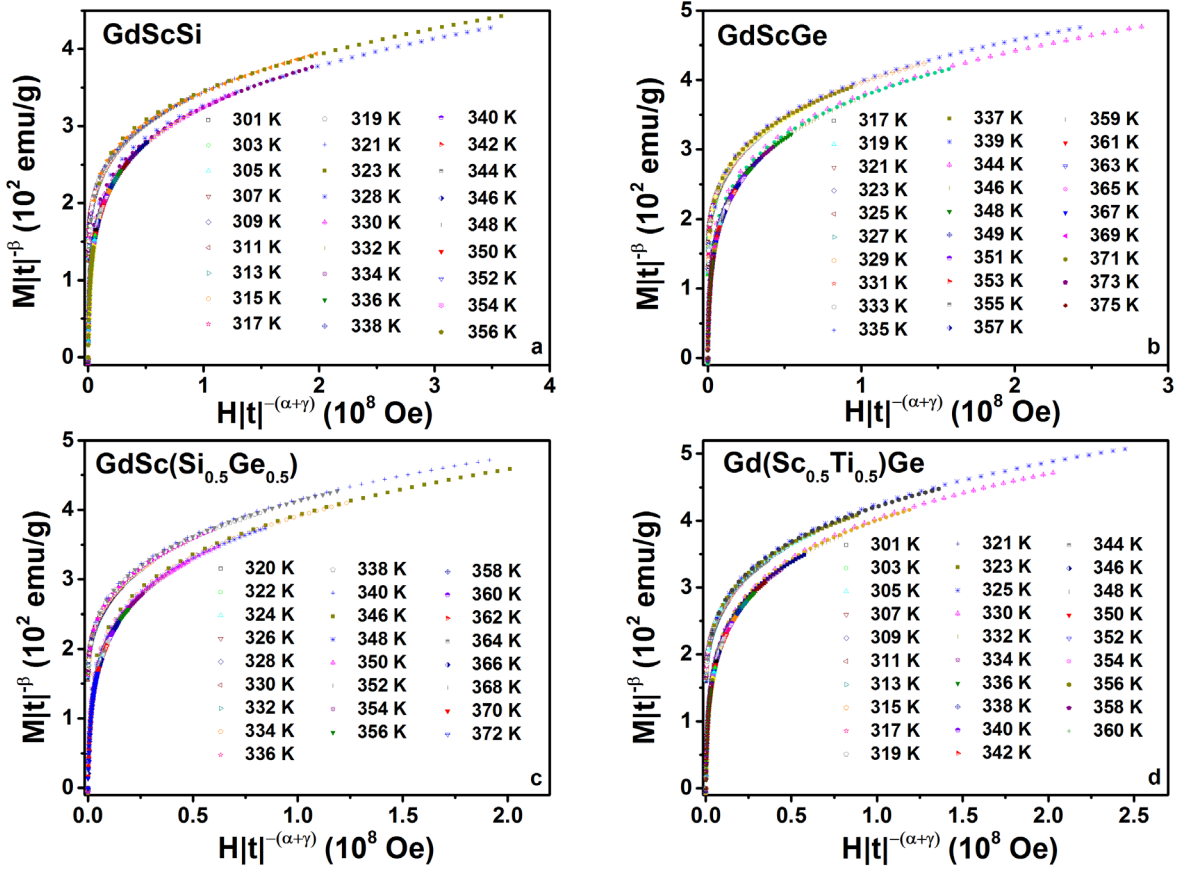
Fig. 7. The renormalized magnetization plotted as a function of the renormalized field following Eq. (5) for GdScSi (a), GdScGe (b), GdSc(Si$_{0.5}$Ge$_{0.5}$) (c), Gd(Sc$_{0.5}$Ti$_{0.5}$)Ge (d). In each case, all data collapse in two separate branches, one above and one below T$_C$. The graphs contain curves with ΔT=1K , though the legends do not show all temperatures.

Finally, the value of the critical exponent α has been independently evaluated through high resolution measurements of the specific heat in the near vicinity of the Curie temperature using an *ac* photopyroelectric calorimeter (as explained in Section 2. Materials and Methods).

The experimental specific heat curves have been fitted to the well known equation:

$$c_p = B + Ct + A^{\pm} \left| t \right|^{-\alpha} \left(1 + E^{\pm} \left| t \right|^{0.5} \right) \qquad (8)$$

where $t=(T-T_C)/T_C$ is the reduced temperature and α, $A^{\pm}$, B, C and $E^{\pm}$ are adjustable parameters. Superscripts + and - stand for $T > T_C$ and $T < T_C$ respectively. The linear term represents the background contribution to the specific heat, while the last term is the anomalous contribution to the specific heat. The factor under parenthesis is the correction to scaling that represents a singular contribution to the leading power as known from experiments and theory. A non-linear least square routine using a Levenberg-Marquardt method has been used to simultaneously fit the experimental data for $T > T_C$ and $T < T_C$. The details of the fitting procedure can be found elsewhere [42].

Figs. 8 and 9 show the experimental specific heat curves in the near vicinity of the critical temperature as a function of the reduced temperature, together with the fittings, for the four compositions. In each case, a deviation plot is also included, showing the difference between the experimental and fitted curves, as a percentage. The fitting is quite good in all cases and the obtained parameters α and A^+/A^- have been included in Table 2. The sign and value of α agrees very well with the 3D-Heisenberg model (for which the theoretical value is -0.134), while the ratio A^+/A^- agrees well for GdScGe and GdSc(Si$_{0.5}$Ge$_{0.5}$) but shows some deviation in the case of GdScSi, and Gd(Sc$_{0.5}$Ti$_{0.5}$)Ge.
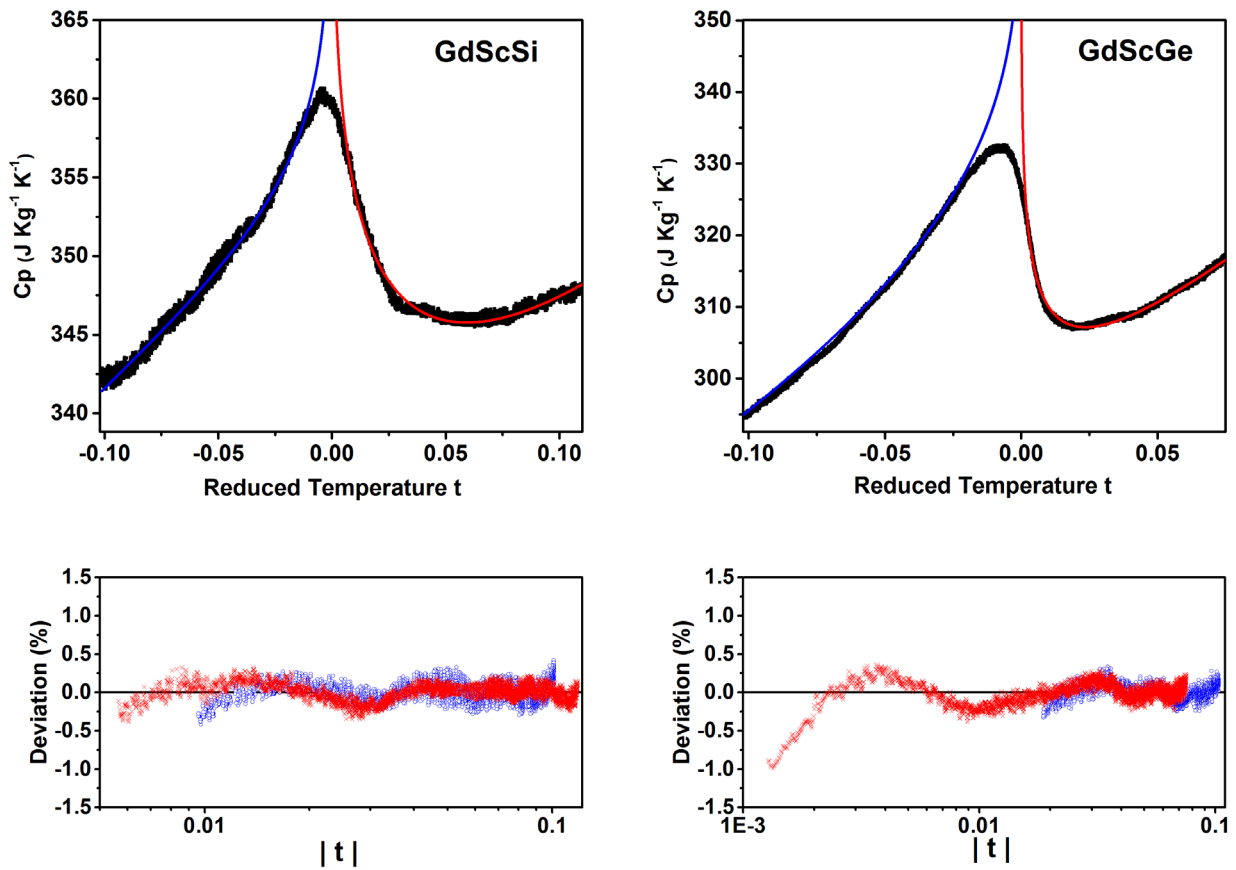

Fig. 8. Experimental (dots) and fitted curves (continuous lines) of the specific heat as a function of the reduced temperature for GdScSi (left), GdScGe (right) in the near vicinity of T_C (top); deviation plots for the fittings (bottom). Open circles are for $T < T_C$, crosses for $T > T_C$.
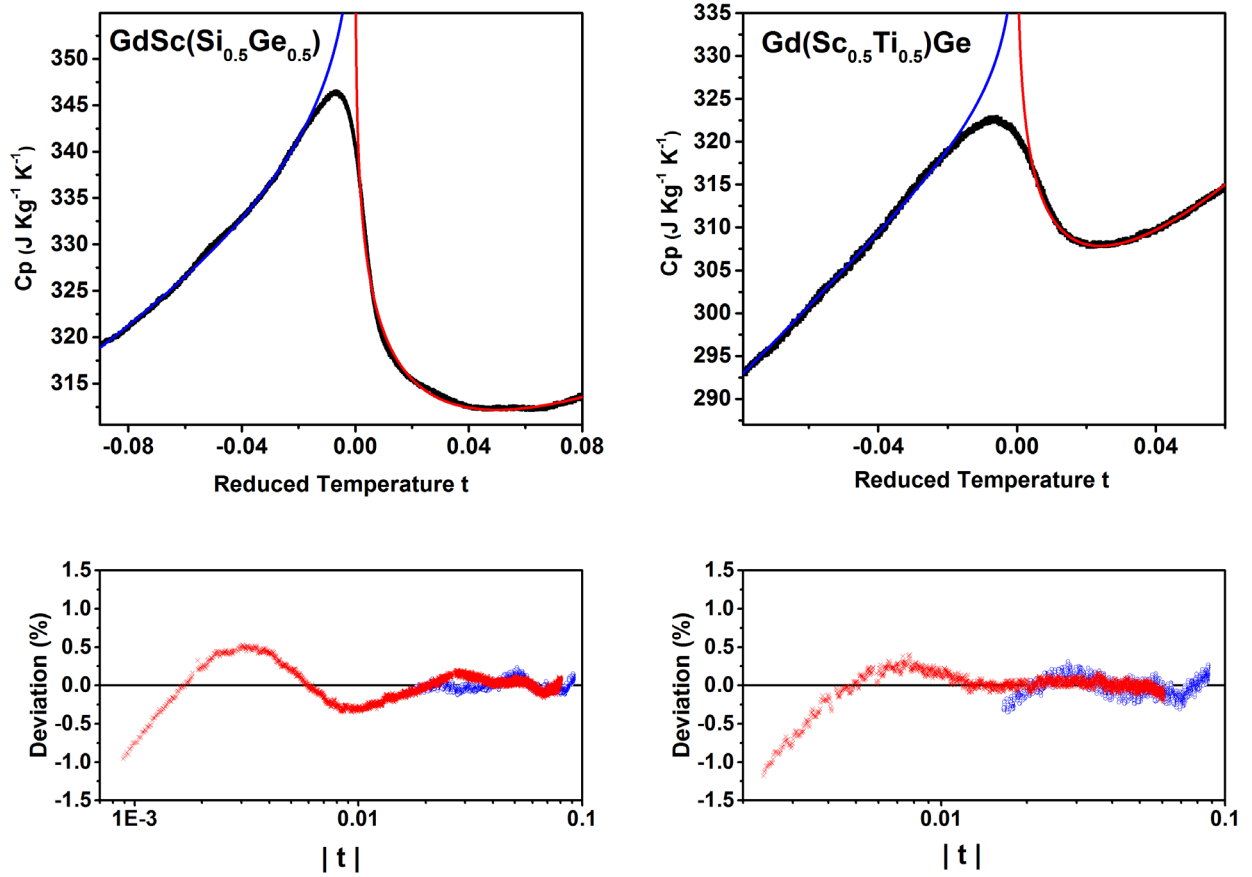
Fig. 9. Experimental (dots) and fitted curves (continuous lines) of the specific heat as a function of the reduced temperature for GdSc(Si$_{0.5}$Ge$_{0.5}$) (left), Gd(Sc$_{0.5}$Ti$_{0.5}$)Ge (right) in the near vicinity of T$_C$ (top); deviation plots for the fittings (bottom). Open circles are for T < T$_C$, crosses for T > T$_C$.

4. Discussion

One main issue regarding the properties of these Gd-based intermetallic compounds is the fact that their Curie temperature is higher than that of the Gd metal alone (which is 294 K [12]) by more than 50 K. It is now clear that the ferromagnetic transition is solely due to the ordering of the rare earth spins. The 3d-sublattice of the transition metal (Sc or Ti) does not carry any magnetic moment; it is accepted that this is due to the hybridization of this 3d band with the p band of Si (Ge), leading to a filling of the 3d band [3]. In GdScSi, GdTiGe, GdTiSi, a common mechanism has been suggested to account for the high ordering temperature of the Gd spins. The interaction between f electrons decreases with increasing distance; therefore, a lower transition temperature would be expected when the Gd ions are within the tetragonal CeScSi structure, as there is a larger separation between rare earths [13, 43, 44]. A significant spin polarization of the 3d electrons of the transition metals Sc and Ti has been found in both cases, with a strong hybridization between these electrons and the also spin

14

polarized *5d* band electrons of the rare earth, which would enable an enhancement of the indirect exchange interaction between the rare earth moments through a RKKY mechanism and an increase in the critical temperature [9, 10, 12, 45].

The Curie temperatures obtained in this study for GdScSi and GdScGe are in general agreement with those found in literature [3, 11, 12, 44] though there are some discrepancies about which one has a higher Curie temperature (GdScGe in our case, with nearly the same value than the one given by Manfrinetti [11] and Couillaud [44]). GdSc(Si$_{0.5}$Ge$_{0.5}$) has nearly the same Curie temperature as GeScGe while Gd(Sc$_{0.5}$Ti$_{0.5}$)Ge has a lower one, which is interesting because GdTiGe (in the same CeScSi structure) was reported with a Curie temperature higher than that of GeScGe, of about 25 K [9]. These differences have to do with the effective hybridization between the Gd-*5d* states and the transition metal-*3d* states. In particular, in the case of GdTiSi and GdTiGe it was proved that the substitution of Si by Ge made the *5d-3d* hybridization stronger, resulting in a higher Curie temperature [9]. This allows us to interpret that the effective hybridization between the *d* states must be weaker in Gd(Sc$_{0.5}$Ti$_{0.5}$)Ge than in GdTiGe and GdScGe. Besides, a similar situation arises when comparing GdScSi and GdScGe: the higher critical temperature in the latter is surely due to a stronger *5d-3d* hybridization as a consequence of the change in the *X*-block.

The results of the critical behavior study (summarized in Table 2) allow us to conclude that all four ferromagnetic transitions belong to the 3D-Heisenberg class, presenting isotropic and short-range order magnetic interactions. This is in stark discrepancy with previous results on NdScSi and NdScGe, where it was proved that the first one belongs to the 3D-XY universality class while the second one presented critical exponents close to the mean field model [32]. A further proof that the magnetic properties of Nd and Gd compounds are extremely different. In the first place, the Curie temperature has been raised about 150 K between the compounds with Nd and Gd; secondly, the crystalline electric field anisotropies from localized *4f* states which appear in other rare earth ions, such as Pr and Nd, are not present in Gd [10, 12], thus favoring the non appearance of magnetocrystalline anisotropies which could make the critical behavior deviate from isotropic to planar (3D-XY) or uniaxial (3D-Ising). Nevertheless, there are small deviations in some of the critical parameters from the perfect 3D-Heisenberg universality class. In GdScSi, the ratio of the critical coefficients A^+/A^- is smaller than the theoretical one (1.02 against 1.52); in GdScGe, γ is slightly smaller (1.305 against 1.386), as well as in GdSc(Si$_{0.5}$Ge$_{0.5}$) (1.307 versus 1.386). These are indications that there is not a perfect magnetic isotropy; a result which can be attributed to the fact that there is a non-negligible spin-orbit coupling of the itinerant electrons which could introduce a subtle magnetocrystalline anisotropy, as it happens in pure Gd [46] and has been suggested for GdScGe$_{1-x}$Sb$_x$ [12]. In the analysis of critical behavior in manganites, for instance, these small deviations from perfect 3D-Heisenberg exponents arise often [47-50]. What is clear is that the fact

that the *X*-block in GdSc*X* be Si, Ge or a combination of both does not make much difference in the magnetic properties, even if it must have some influence in the orbitals hybridization; it simply places the transition slightly lower or higher, without however having more than a slight effect on the critical behavior of the transition. Guillou *et al* [12] also found that in $Gd_{1.02}Sc_{0.98}Ge_{1-x}Sb_x$ the magnetic exchange interactions were not directly affected by the substitution of Ge by Sb.

The composition which more evidently deviates from the perfect 3D-Heisenberg is $Gd(Sc_{0.5}Ti_{0.5})Ge$, for which γ is 1.283 and A^+/A^- 1.16 (instead of 1.386 and 1.52), though α and β are in agreement with the Heisenberg model and these last two exponents are always taken as the leading parameters in the attribution of universality classes. As the mechanism of *d*-states hybridization is at the core of the magnetic properties of this intermetallic family, the fact that we have two different transition metals with different state of polarization of their *3d*-spins must surely be responsible for this slight deviations in γ and A^+/A^-.

5. Conclusions

The critical behavior of the ferromagnetic transition in GdScSi, GdScGe, GdSc(Si$_{0.5}$Ge$_{0.5}$) and Gd(Sc$_{0.5}$Ti$_{0.5}$)Ge has been studied by means of calorimetric as well as magnetic techniques. The critical parameters α, β, γ, δ, and A^+/A^- have been independently obtained and they agree with the 3D-Heisenberg universality class, stating that the magnetic interactions are short-range and that the spins are ordered isotropically. The differences in the Curie temperatures among the compositions and certain deviations of the critical parameters from the theoretical values are explained on the basis of the variation of the *d* states hybridization between the rare earth and the transition metal, as well as the presence of small magnetocrystalline anisotropies arising from spin-orbit coupling effects.

REFERENCES

[1]   S. Gupta, K.G. Suresh, J. Alloys Compd. 618 (2015) 562-606.

[2]   S. Singh, S.K. Dhar, C. Mitra, P. Paulose, P. Manfrinetti, A. Palenzona, J. Phys.: Condens. Matter 13 (2001) 3753-3766.

[3]   S.A. Nikitin, I.A. Ovtchenkova, Yu.V. Skourski, A.V. Morozkin, J. Alloys Compd. 345 (2002) 50-53.

[4]   S.N. Mishra, S.K. Dhar, J. Phys.: Condens. Matter 16 (2004) 635-640.

[5]   S. Singh, S.K. Dhar, P. Manfrinetti, A. Palenzona, D. Mazzone, J. Magn. Magn. Mater. 269 (2004) 113-121.

[6]   J.M. Cadogan, D.H. Ryan, R. Gagnon, C.J. Voyer, J. Appl. Phys. 97 (2005)   10A916.

[7]   P. Manfrinetti, A.V. Morozkin, O. Isnard, P. Henry. A. Palenzona, J. Alloys Compd. 450 (2008) 86-91.

[8]   P.D. Kulkarni, U.V. Vaidya, S.K. Dhar, P. Manfrinetti, A.K. Grover, J. Phys. D: Appl. Phys. 42 (2009) 082001 (5 pp).

[9]   G. Skorek, J. Denyszczyk, J. Szade, B. Tyszka, J. Phys.: Condens. Matter 13 (2001) 6397-6409.

[10] S.N Mishra, J. Phys.: Condens. Matter 21 (2009) 115601 (11pp).

[11] P. Manfrinetti, M. Pani, A. Palenzona, S.K. Dhar, S. Singh, J. Alloys Compd. 334 (2002) 9-13.

[12]   F. Guillou, A.K. Pathak, T.A Hackett, D. Paudyal, Y. Mudryk, V.K. Pecharsky, J. Phys.: Condens. Matter 29 (2017) 485802 (10pp).

[13]   A.V. Morozkin, L.M. Vitting, I.A. Sviridov, I.A. Tskhadadze, J. Alloys Compd. 297 (2000) 168-175.

[14] S.A. Nikitin, I.A. Tskhadadze, I.V. Telegina, A.V. Morozkin, Yu.D. Seropegin, J. Magn. Magn. Mater. 182 (1998) 375-380.

[15] H.E. Stanley, "Introduction to phase transitions and critical phenomena", Oxford University Press (1971).

[16] R. Guida, J. Zinn-Justin, J. Phys. A: Math. Gen. 31 (1998) 8103-8121.

[17] M. Campostrini, M. Hasenbusch, A. Pelissetto, P. Rossi, E. Vicari, Phys. Rev. B 63 (2001) 214503.

[18] M. Campostrini, M. Hasenbusch, A. Pelissetto, P. Rossi, E. Vicari, Phys. Rev. B 65 (2002) 144520.

[19] M. Hasenbusch, Phys. Rev. B 82 (2010) 174434.

[20] K. Yvon, W. Jeitschko and E. Parthe´, J. Appl. Crystallogr. 10 (1977) 73–74.

[21] S.K. Dhar, P. Manfrinetti, A. Palenzona, M. Pani, J. Alloys Compd. 347 (2002) 1–8.

[22] W. Jiang, X.Z. Zhou, G. Williams, Y. Mukovskii, K. Glazyrin, Phys. Rev. B 78 (2008) 144409.

[23] W. Jiang, X.Z. Zhou, G. Williams, Y. Mukovskii, K. Glazyrin, Phys. Rev. B 77 (2008) 064424.

[24] U. Zammit, M. Marinelli, F. Mercuri, S. Paoloni, F. Scudieri, Rev. Scient. Inst. 82 (2011) 121101.

[25] U. Zammit, M. Marinelli, F. Mercuri, S. Paoloni, J. Phys. Chem. B 113 (2009) 14315-14322.

[26] U. Zammit, S. Paoloni, F. Mercuri, M. Marinelli, F. Scudieri, AIP Advances 2 (2012) 012135.

[27] A. Oleaga, V. Shvalya, V. Liubachko, G. Balakrishnan, L.D. Tung, A. Salazar, J. Alloys Compd. 703 (2017) 210-215.

[28] A. Oleaga, V. Shvalya, A. Salazar, I. Stoika, Yu.M. Vysochanskii. J. Alloys Compd. 694 (2017) 808-814.

[29] A. Oleaga, A. Salazar, D. Skrzypek, J. Alloys Compd. 629 (2015) 178-183.

[30] M. Massot, A. Oleaga, A. Salazar, D. Prabhakaran, M. Martin, P. Berthet, G. Dhalenne, Phys. Rev. B 77 (2008) 134438.

[31] A. Herrero, A. Oleaga, A. Salazar, A.F. Gubkin, N.V. Baranov, J. Alloys Compd. 741 (2018) 1163-1168.

[32] A. Oleaga, V. Liubachko, P. Manfrinetti, A. Provino, Yu. Vysochanskii, A. Salazar, J. Alloys Compd. 723 (2017) 559-566.

[33] A. Salazar, Rev. Sci. Instrum. 74 (2003) 825.

[34] A.O. Oliynyk, T.D. Sparks, M.W. Gaultois, L. Ghadbeigi, A. Mar, Inorganic Chem. 55 (2016) 6625-6633.

[35] A.K. Bashir, M.B.T. Tchokonté, A.M. Strydom, J. Magn. Magn. Mater. 414 (2016) 69-73.

[36] A. Oleaga, A. Salazar, D. Prabhakaran, A.T. Boothroyd, Phys. Rev. B 70 (2004) 184402.

[37] A. Oleaga, A. Salazar, H. Kuwahara, Physica B 378-380 (2006) 512-514.

[38] S.K. Banerjee, Phys. Lett. 12 (1964) 16.

[39] A. Oleaga, A. Salazar, M. Ciomaga Hatnean, G. Balakrishnan, Phys. Rev. B 92 (2015) 024409.

[40] A.K. Pramanik, A. Banerjee, Phys. Rev. B 79 (2009) 214426.

[41] J.S. Kouvel, M.E. Fisher, Phys. Rev. 136 (1964) A1626.

[42] A. Oleaga, A. Salazar, D. Prabhakaran, J.G. Cheng, J.S. Zhou, Phys. Rev. B 85 (2012) 184425.

[43] A.V. Morozkin, Yu.D. Seropegin, V.K. Portnoy, A.V. Leonov, I.A. Sviridov, J. Alloys Compd. 278 (1998) L1-L5.

[44] S. Couillaud, E. Gaudin, V. Franco, A. Conde, R. Pöttgen, B. Heying, U.Ch. Rodewald, B. Chevalier, Intermetallics 19 (2011) 1573-1578.

[45] C. Ritter, S.K. Dhar, R. Kulkarni, A. Provino, D. Paudyal, P. Manfrinetti, K.A. Gschneidner, J. Phys.: Condens. Matter 26 (2014) 366001 (13pp).

[46] M. Colarieti-Tosti, T. Burkert, O. Eriksson, L. Nordström, M.S.S. Brooks, Phys. Rev. B 72 (2005) 094423.

[47] A. Oleaga, A. Salazar, D. Prabhakaran, A.T. Boothroyd, J. Phys.: Condens. Matter 17 (2005) 6729-6736.

[48] J. Yang, Y.P. Lee, Appl. Phys. Lett. 91 (2007) 142512.

[49] N. Mtiraoui, J. Dhahri, M. Oumezine, J. Magn. Magn. Mater. 345 (2013) 118-124.

[50] N. Ghosh, S. Rößler, U.K. Rößler, K. Nenkov, S. Elizabeth, H.L. Bhat, K. Dörr, K.H. Müller, J. Phys.: Condens. Matter 18 (2006) 557-567.

FIGURE CAPTIONS

Fig. 1 Thermal diffusivity as a function of temperature for GdScSi (■), GdScGe (▲), GdSc(Si$_{0.5}$Ge$_{0.5}$) (♦), Gs(Sc$_{0.5}$Ti$_{0.5}$)Ge (●). Not all points are shown, for the sake of clarity.

Fig. 2. Magnetization as a function of temperature for GdScSi (■), GdScGe (▲), GdSc(Si$_{0.5}$Ge$_{0.5}$) (♦), Gs(Sc$_{0.5}$Ti$_{0.5}$)Ge (●) using a magnetic field of 100 Oe.

Fig. 3. (a) Arrott Plot and (b) Modified Arrott Plot of the isotherms collected around T_C for GdScGe, with the Heisenberg trial exponents showing the parallelism of the linear fittings at high fields.

Fig.4. Spontaneous magnetization (left) and inverse of initial susceptibility (right) vs. temperature for GdScSi (a), GdScGe (b), GdSc(Si$_{0.5}$Ge$_{0.5}$) (c), Gd(Sc$_{0.5}$Ti$_{0.5}$)Ge (d), as obtained from the optimized Modified Arrot Plot. The solid curves correspond to the fits to Eq. (2) and (3), as explained in the text.

Fig. 5. Kouvel-Fisher plot of spontaneous magnetization (left) and inverse of initial susceptibility (right) for GdScSi (a), GdScGe (b), GdSc(Si$_{0.5}$Ge$_{0.5}$) (c), Gd(Sc$_{0.5}$Ti$_{0.5}$)Ge (d). The straight lines are linear fits, from which T$_C$ and the critical exponents are obtained.

Fig. 6. *M* vs. *H* plot in a log-log scale collected at critical isotherms for GdScSi (a), GdScGe (b), GdSc(Si$_{0.5}$Ge$_{0.5}$) (c), Gd(Sc$_{0.5}$Ti$_{0.5}$)Ge (d). The straight line is the linear fit from which the exponent δ is obtained.

Fig. 7. The renormalized magnetization plotted as a function of the renormalized field following Eq. (5) for GdScSi (a), GdScGe (b), GdSc(Si$_{0.5}$Ge$_{0.5}$) (c), Gd(Sc$_{0.5}$Ti$_{0.5}$)Ge (d). In each case, all data collapse in two separate branches, one above and one below T$_C$. The graphs contain curves with ΔT=1 K , though the legends do not show all temperatures.

Fig. 8. Experimental (dots) and fitted curves (continuous lines) of the specific heat as a function of the reduced temperature for GdScSi (left), GdScGe (right) in the near vicinity of T$_C$ (top); deviation plots for the fittings (bottom). Open circles are for T < T$_C$, crosses for T > T$_C$.

Fig. 9. Experimental (dots) and fitted curves (continuous lines) of the specific heat as a function of the reduced temperature for GdSc(Si$_{0.5}$Ge$_{0.5}$) (left), Gd(Sc$_{0.5}$Ti$_{0.5}$)Ge (right) in the near vicinity of T$_C$ (top); deviation plots for the fittings (bottom). Open circles are for T < T$_C$, crosses for T > T$_C$.

Table 1. Main universality classes for different magnetic systems [15-19].

Universality class	α	β	γ	δ	A^+/A^-
Mean-field Model	0	0.5	1.0	3.0	-
3D-Ising	0.11	0.3265	1.237	4.79	0.53
3D-XY	-0.014	0.34	1.30	4.82	1.06
3D-Heisenberg	-0.134	0.365	1.386	4.80	1.52

Table 2. Values of the obtained critical exponents and parameters β, γ, δ, α, and A^+/A^-.

Material	Technique	β	γ	δ	α	A^+/A^-
GdScSi	Modified Arrott Plot	0.3617 ±0.0005 T_C=325.41 ± 0.01 K	1.384 ±0.004 T_C =325.56 ± 0.05 K	4.83 [a] ±0.02		
	Kouvel-Fisher Method	0.360 ±0.004 T_C=325.36 ± 0.03 K	1.375 ±0.007 T_C=325.60 ± 0.06 K	4.82 [a] ±0.06		
	Critical Isotherm			4.86 ± 0.02		
	Photopyroelectric calorimetry				-0.120 ±0.020	1.02 ±0.13
GdScGe	Modified Arrott Plot	0.3688 ±0.0004 T_C=341.43 ± 0.01 K	1.301 ±0.004 T_C=341.87 ± 0.05 K	4.53 [a] ±0.02		
	Kouvel-Fisher Method	0.372 ±0.003 T_C=341.48 ± 0.03 K	1.305 ±0.005 T_C=341.75 ± 0.06 K	4.51 [a] ±0.04		
	Critical Isotherm			4.799 ±0.006		
	Photopyroelectric calorimetry				-0.134 ±0.005	1.63 ±0.07
GdSc(Si$_{0.5}$Ge$_{0.5}$)	Modified Arrott Plot	0.369 ±0.001 T_C=342.88 ± 0.01K	1.306 ±0.004 T_C =343.22 ± 0.04 K	4.54[a] ±0.02		
	Kouvel-Fisher Method	0.372 ±0.002 T_C=342.95 ± 0.03 K	1.307 ±0.005 T_C=343.14 ± 0.05 K	4.52 [a] ±0.03		
	Critical Isotherm			4.813 ±0.006		
	Photopyroelectric calorimetry				-0.135 ±0.007	1.56 ±0.07
Gd(Sc$_{0.5}$Ti$_{0.5}$)Ge	Modified Arrott Plot	0.370 ±0.001 T_C=327.16 ± 0.01 K	1.283 ±0.004 T_C =327.59 ± 0.06 K	4.47 [a] ±0.02		
	Kouvel-Fisher Method	0.370 ±0.004 T_C=327.13 ± 0.03 K	1.282 ±0.005 T_C=327.55 ± 0.07 K	4.47 [a] ±0.05		
	Critical Isotherm			4.802 ±0.002		

Photopyroelectric calorimetry	-0.122 ±0.010	1.16 ±0.08

[a] Calculated from Eq. (6) $\delta = 1 + \gamma/\beta$.